# Biphasic, Switch-Like Isothermal DNA Amplification

Burcu Özay*, Cara M Robertus*, Jackson L Negri, Stephanie E McCalla
*authors contributed equally to this work
Montana State University, Department of Chemical and Biological Engineering

## Significance Statement

Switch-like reactions are common in the natural world; they are vital to basic cellular operations such as signaling and genetic regulation. These responses are difficult to reproduce in synthetic biological systems, particularly for low concentrations of input molecules such as those seen *in vivo*. We have developed the first reported biphasic DNA amplification reaction, with the second amplification phase giving up to two orders of magnitude greater output than a standard oligonucleotide amplification reaction. Both reaction phases feature tunable kinetics based on DNA association thermodynamics, and the second phase can be tuned to produce ultrasensitive, switch-like signal output. This one-step isothermal reaction can potentially impact a variety of disciplines such as synthetic biology, biosensors, DNA computing, and clinical diagnostics.

## Abstract

Switches are common in biological systems due to their ability to give a definitive response to a specific target molecule in the presence of high concentration background. Synthetic systems aim to reproduce this effect for applications from DNA computing to molecular diagnostics. Exciting new systems can produce switch-like behavior, but typically respond to nanomolar input of target molecule. We report a novel DNA amplification chemistry that has two switch-like characteristics. First, the chemistry is biphasic, with a low-gain first phase and plateau followed by a high gain burst of signal. Second, the reaction kinetics can be tuned to give a large ultrasensitive jump in signal during the second phase. Reaction output at each stage can be rationally tuned based on DNA association thermodynamics. The chemistry is one-step, isothermal, and can be adapted to respond to a broad range of input target molecules. This biphasic DNA amplification reaction could potentially impact diagnostics, DNA circuits, or other sensor systems that require definitive digital outputs.

## Introduction

Switch-like responses to input stimuli are ubiquitous in nature. This switching behavior is common in cell signaling, transcription, and genetic regulatory networks; it is commonly accepted that these switches react decisively to a true signal while filtering out noise[1]. These biological switches typically have two defining characteristics: the first is a definitive "on" and "off" state, and the second is a large ultrasensitive jump in output when above a threshold input. Ultrasensitivity can stem from a variety of mechanisms[2] such as molecular titration[3], sponging[4], multistep signaling[5], homo-multimerization[6], zero-order ultrasensitivity[7], or cooperativity[8,9]. Researchers are using these mechanisms to create biomimetic switches, as they have noted the utility of ultrasensitive amplification kinetics in biosensors, genetic logic gates, DNA circuits, and materials that are required to be highly responsive[10-12].

Several studies have reported switch-like behavior in synthetic biochemical systems. Ion channels can be repurposed into biosensor switches by preventing channel dimerization in the presence of an target antigen, thus turning on in the presence of target[13]. DNA oscillators can switch between an "on" and "off" state by combining DNA degradation with a DNA amplification reaction[14]. The authors noted that the oscillatory effect could be achieved through non-linear DNA amplification instead of non-linear DNA degradation, but the former is currently difficult to obtain and manipulate. Structure-switching sensors such as aptamers[15] and molecular beacons[16,17] change conformation in the presence of a specific target molecule. When properly designed, structure-switching biosensors can also create Hill-type ultrasensitive kinetics: biosensors with two cooperative binding sites produce an ultrasensitive response if the affinity of the target for the second site is altered by target association to the first site[11,12]. These exciting biomimetic systems can stably produce simple, digital (yes/no) outputs with nanomolar trigger inputs, but they have not yet been designed for low input target

concentrations. A single cell can contain as few as 10 miRNA molecules per cell[18], and clinically relevant DNA and RNA concentrations range from hundreds of picomolars to attomolar in range[19]. Clinically relevant protein concentrations are often in the femtomolar range[20]. While previous studies explored sensors that turn on and off with ultrasensitive Hill-type kinetics or created controlled switches, they do not have the subsequent high-gain amplification required for biologically relevant target concentrations.

We present a simple, tunable nucleic acid amplification method with an endogenous switching mechanism. The method takes advantage of a naturally occurring stall in the amplification reaction, which produces a low-level signal. Upon surpassing a threshold, the reaction enters a high-gain second phase "burst", producing a signal that ranges from ten to one hundred times the base DNA amplification reaction. We hypothesize that cooperative opening of a stable looped DNA template creates the high-gain burst. Output kinetics can be tuned to create an ultrasensitive jump that resembles a definitive switch turn-on. The reaction is isothermal and rapid, with a sub-picomolar limit of detection for input trigger DNA.

## Results and Discussion

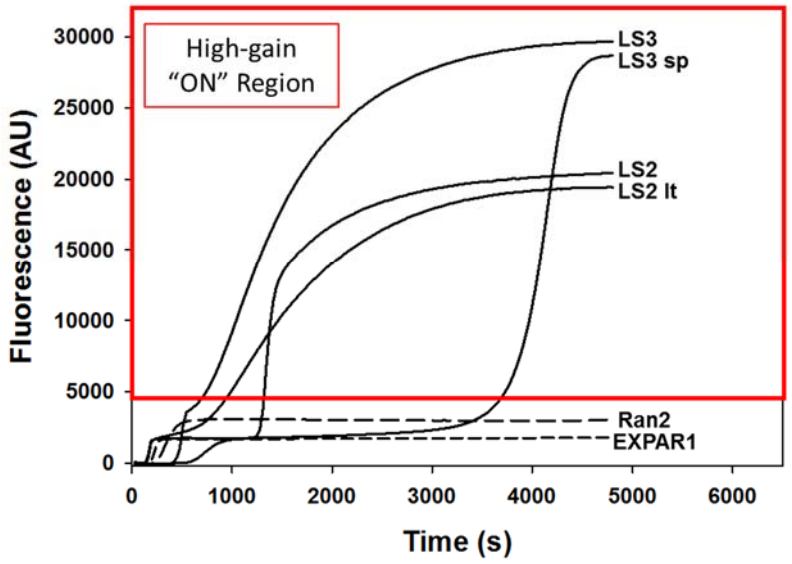


**Figure 1: Representative biphasic amplification reaction output.** DNA amplification output is correlated to fluorescence, which increases and plateaus at approximately the same level as previously reported optimized EXPAR reactions[21,22]. Biphasic DNA amplification output is shown in solid lines, with previously reported EXPAR amplification output shown in dotted lines. After a lag period, the DNA output jumps into a high gain "on" region with tunable kinetics. Template DNA names are labeled next to corresponding output traces; template sequences can be found in the Table SI 1.

*Output and proposed mechanisms of the biphasic DNA amplification reaction*

The biphasic DNA amplification reaction contains the same base components as the exponential amplification reaction for oligonucleotides (EXPAR)[23]. Both EXPAR and the biphasic DNA amplification reaction amplify a trigger sequence of ten to twenty base pairs in length at a single reaction temperature of 55°C through the action of a thermophilic polymerase and a nicking endonuclease. Both reactions will nonspecifically create product in the absence of initial DNA trigger. The main difference between the original EXPAR reaction and the biphasic oligonucleotide amplification reaction is the palindromic sequence within the DNA template that causes the template to fold into a looped configuration. The thermodynamics of the trigger binding and DNA association are in a regime that creates a biphasic DNA amplification reaction; EXPAR-type DNA amplification using looped templates are found in literature[24-26], but the biphasic ultrasensitive kinetics have not yet been reported. Details on the reaction setup are given in the Materials and Methods (Supplementary Information).

The output from the novel biphasic oligonucleotide amplification reaction is shown in Figure 1. Despite the similarities in reaction components, the biphasic amplification reaction reported here is functionally distinct from all other EXPAR reactions. The first phase of the reaction resembles traditional EXPAR output, with an initial rise and a first plateau. Thermodynamics of the looped DNA template and trigger association are well correlated with the first-phase reaction kinetics (Spearman's R = 0.8022, Figure SI 1) when compared to the original EXPAR reaction (R = 0.4072)[21]. This is likely due to the closed template loop; thermodynamics of DNA association dominate the reaction kinetics, contrasting the sequence dependence seen in traditional EXPAR. After the first plateau, the biphasic reaction enters a high-gain second phase. This finding reveals that EXPAR can recover from the first plateau, a fact that was previously unknown. The one template that favors a linear configuration at the reaction temperature (LS3 lowpG2, $T_m$ = 49.2°C) still shows biphasic reaction kinetics, implying that a stable loop structure is not necessary for biphasic amplification.

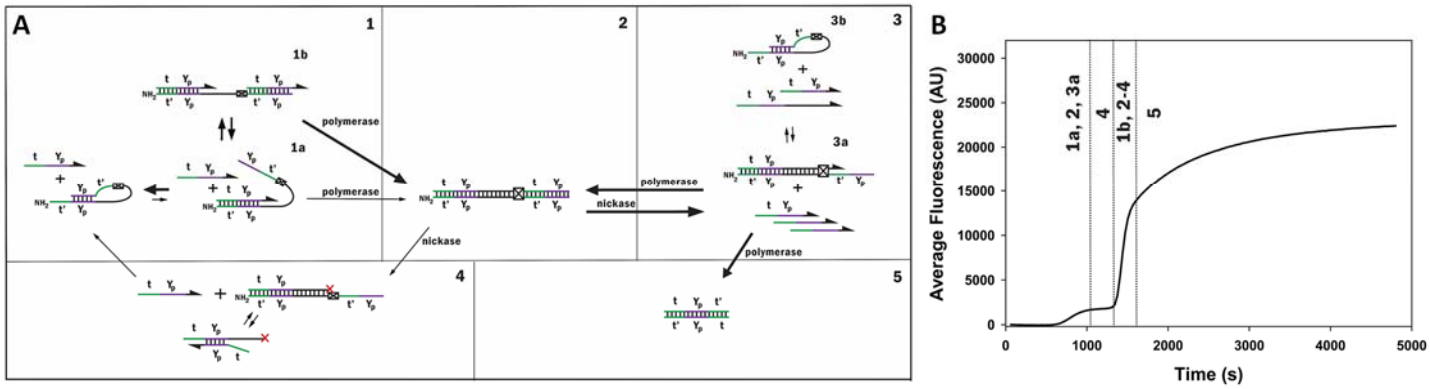


**Figure 2: Biphasic DNA amplification reaction.** (A) The cartoon depicts potential reaction pathways in the biphasic DNA amplification reaction. The amplification requires a looped DNA template with two palindromic sequences ($Y_p$), two toeholds (t'), and a restriction site (⊠), as well as polymerase and nickase enzymes. The reaction amplifies a DNA trigger with a reverse compliment to the template toehold (t) and the palindromic region ($Y_p$); arrows show extendable 3' ends of the DNA. The trigger can bind to either toehold region t' and strand displace the palindromic region $Y_p$, thus opening the loop (1). A polymerase can then extend the trigger and create the recognition site for a nicking endonuclease (2), as well as an identical trigger. The nickase then cuts the top strand (3a), freeing the newly created trigger to bind other templates (1). The loop can also remove the long trigger and close with the aid of short triggers, which can bind the long trigger and facilitate loop closure (3b, 4). This may be vital to remove "poisoned" long triggers that cannot amplify and block further trigger amplification on the template (4). The palindromic region can also cause trigger dimerization, after which the toehold regions can be filled by the polymerase; this removes trigger molecules from further amplification cycles (5). (B) A representative reaction trace of template LS2; the reaction stages are labeled with proposed reaction mechanisms that govern each stage.

The mechanism behind the switch-like oligonucleotide amplification reaction is likely driven by multiple phenomena, as shown in Figure 2a. The DNA template is composed of two copies of the complementary sequence joined by a nine nucleotide nicking enzyme recognition site, specifically containing: a 3' amine group to prevent extension of the template, a 3' toehold, a palindromic sequence, the nickase recognition site, the repeated 5' toehold, and the repeated palindromic sequence (1). The palindromic region causes the template to fold into a looped configuration. Triggers for these templates consist of the toehold complement and the template palindrome. When a trigger binds to the 3' end of the template, the DNA polymerase extends the strand and the nicking enzyme recognition site is created (2). The nickase then nicks the growing strand (3a). The polymerase extends at this nick and strand displaces the downstream trigger (3a → 2). The displaced trigger is then free to prime other templates, leading to exponential amplification (3a → 1). The amplification therefore produces both triggers and long triggers that contain the nickase recognition site on their 3' end (3b). The presence of the palindromic sequence produces several new reaction pathways. The palindromic section of the triggers can associate, be extended by the polymerase, and create inert triggers unable to further replicate; this pathway has been previously discussed[24] (5). The trigger can catalyze removal of the long, stable trigger by binding to either the palindromic region of the long trigger or by binding to the template (3b, 4). Loop closure will also aid in removal of trigger and long

trigger from the template. Finally, the presence of the loop with two toehold regions creates cooperative binding between the triggers and the looped template. For most templates, the looped configuration is more stable than the open, trigger-bound configuration (Table SI 2). The association of the template and the first trigger molecule will open the loop, which both aids and stabilizes a second trigger association (1b). We hypothesize that these new reaction pathways create the unique features of our amplification reaction detailed in Figure 2b.

*Properties of the first reaction phase*

The first reaction phase resembles the base EXPAR reaction, with a rapid, low-gain reaction phase followed by a plateau. While this stall was previously attributed to loss of nickase integrity, the recovery of the reaction after the first plateau invalidates this theory. Recently others have hypothesized that some templates could be "poisoned" due to polymerase errors that render the DNA strand bound to the template unextendible (Figure 2a, panel 5)[27]. We hypothesize that this could cause the plateau seen in the original EXPAR reaction and the first plateau in the biphasic amplification reaction (Figure 1). We estimated the plateau trigger concentration to be on the order of 1 μM (Figure SI 2), which ten times greater than the template concentration. Due to the rapid template inactivation after ten cycles of extension and nicking it is unlikely that polymerase error causes this plateau, given error rates of polymerases such as *Bst* DNA polymerase that lack the 3′ → 5′ exonuclease domain are approximately $10^{-4}$ [28]. We hypothesize that the plateau is due to noncanonical behavior of the nickase enzyme that leaves a long unextendible trigger (Figure 2a panel 4), as the nickase is operating in suboptimal conditions when compared to the polymerase[22]. It is also possible that a fully elongated trigger poisons the template; the mechanism behind the template poisoning is beyond the scope of this study.

*Properties of the second reaction phase*

After the first plateau, the amplification enters a high-gain second phase followed by a second plateau. The second plateau is caused by exhaustion of reaction components and a buildup of inhibitory reaction byproducts. This effect of inhibitory products was previously described when using EXPAR reactions and a palindromic looped template[24]. Many of the templates exhibit Hill-like ultrasensitive second phase kinetics, marked by a large jump in reaction product that greatly exceeds first phase reaction kinetics. We hypothesize two mechanisms that may contribute to this jump. First, the removal of the long trigger can theoretically be aided by trigger association to the long "poisoned" triggers (Figure 1, panel 4). This would also prevent the long trigger from reassociating with the template, particularly after polymerase extension of the 3' trigger end. The trigger could also dynamically bind the template preventing reassociation of the long trigger. These events would aid in the loop closure and template recycling. This rescue of the poisoned templates allows the reaction to produce 10-100 times more endpoint reaction product, as measured by calibrated SYBR II fluorescence (Supplementary Information). Endpoint product concentration ranged from 7.8 – 116.9 μM, with several reaction products exceeding 100 μM during the second plateau (Table SI 3). Second, the trigger can bind either toehold as seen in Figure 1 panel 1. As the loop is stable when compared to the trigger:template association (Table SI 2), the accumulation of reaction products would produce more open loops and give nonlinear reaction kinetics $\left({}^{d([trigger])}/_{dt} \propto [trigger]^2\right)$. The final output of the second phase is approximately the size of the DNA triggers as seen in PAGE analysis of reaction products; for more details see the Supplementary Information (Figure SI 3).

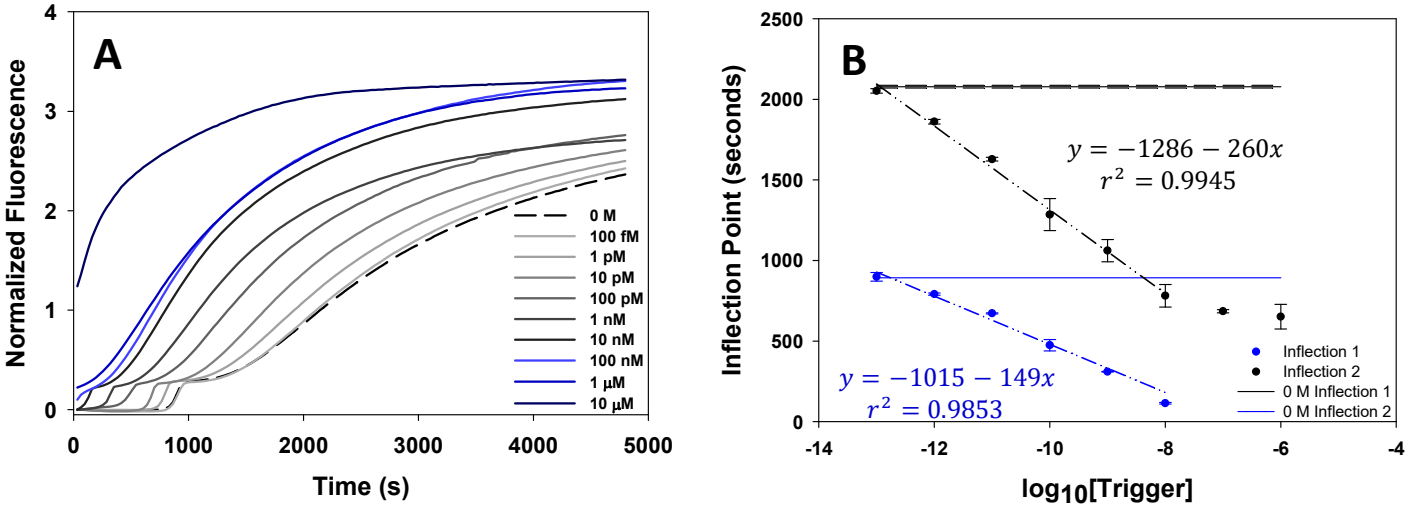


**Figure 3: Correlation between onset of amplification and trigger oligonucleotide concentration.** (A) The real-time reaction output for a representative template LS3 lrs-4 shows the dependence of the reaction on initial trigger concentration, with fluorescence correlated to the produced DNA trigger. Blue traces did not have measurable first reaction phases; high concentrations of trigger (≥1 µM) bypass the first reaction phase entirely, implying that the plateau of this template is on the order of [trigger] = 1 µM. (B) The inflection points are experimental triplicates, and the dotted lines are linear fits. The solid lines show inflection point of the negative control (0 M initial trigger concentration), with surrounding dashed lines showing the standard deviation of the negative control inflection point (not visible for the second inflection point, ± 1.8 s). The first inflection points vary linearly with the log of initial trigger concentration, and the second inflection points vary linearly with the log of initial trigger concentration when initial trigger concentration is ≤ 10 nM. Error bars represent experimental triplicates.

*Reaction response to initial trigger concentration*

We measured reaction output in real-time with varying initial trigger concentrations using the ssDNA binding dye SYBR II for fluorescent readout. Figure 3a shows the average of three real-time fluorescent traces with varying initial trigger concentrations normalized to the fluorescence at the second inflection point. The first and second inflection points correspond to the times at which maximum first derivative of the fluorescence occur for the first and second reaction phase (Figure SI 4). Inflection points are traditionally used as a surrogate for EXPAR reaction kinetics. The first reaction phase was not present for high trigger concentrations ≥ 1 µM, which was the approximate concentration of reaction products quantified during the plateau phase of a biphasic amplification reaction (Figure SI 2). High concentrations of trigger appeared to prevent the reaction from entering the plateau phase, which suggested that entering the second reaction phase is dependent on trigger concentration or rate of trigger production. The inflection points of the first phase linearly correlated to the log of the initial trigger concentration, which is also true of EXPAR reactions[22] (Figure 3b). The second phase inflection points also linearly correlated with the log of the initial trigger concentration for low initial concentrations of trigger (≤ 10 nM). As with traditional EXPAR, the limit of detection for the DNA trigger was determined by the nonspecific amplification rates; the reaction in Figure 3 has a sub-picomolar limit of detection, and nearly all templates reported here could distinguish between 0 and 10 pM initial trigger concentrations (Figure SI 5).

*Varying toehold thermodynamics within templates*

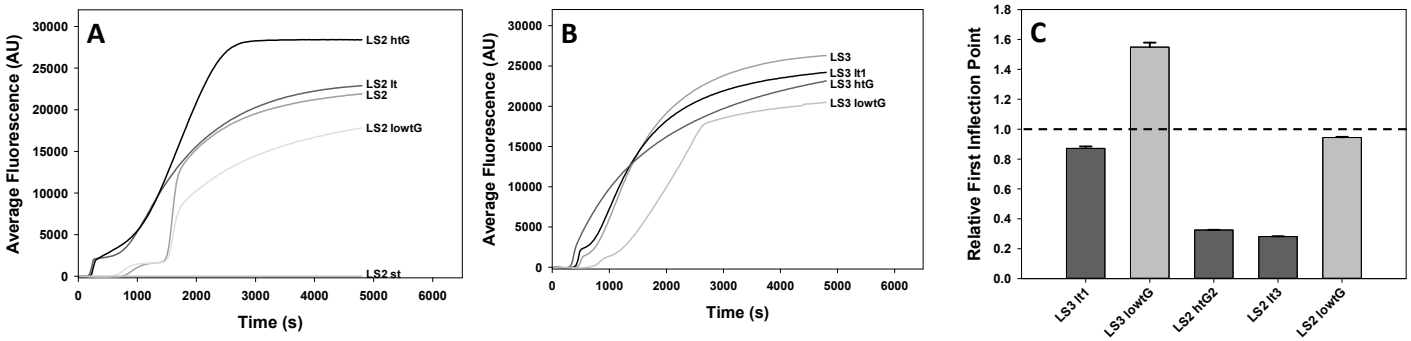


**Figure 4: Effect of toehold free energy on template performance.** (A) Amplification curves of LS2 toehold variants, with the strongest toeholds in black and weaker toeholds in lighter shades of grey. (B) Amplification curves of LS3 toehold variants, with stronger toeholds in black and weaker toeholds in lighter shades of grey. (C) The templates shown in the bar graph are in order from strongest to weakest toehold free energies with respect to the base template (LS2 or LS3). Darker bars have stronger toeholds than the base templates, lighter bars have weaker toeholds than the base template, and the dotted lines show an inflection point equal to the base template. The relative first inflection point is the time of the first inflection point divided by the first inflection point of the base templates LS2 or LS3.

We varied individual thermodynamic parameters of the templates to examine the relative contributions of each parameter to reaction output, and to determine if the biphasic DNA amplification reaction could be rationally tuned by manipulating DNA association thermodynamics. We varied toehold free energy by changing the length or GC content of the template and trigger toehold region. For both LS2 (Figure 4A) and LS3 (Figure 4B), increasing the length of the toehold generally causes the loop to open more rapidly, thus lowering the first phase inflection point. This again demonstrated that template thermodynamics could be manipulated to alter the kinetics of the first reaction phase. LS2 lowtG had a lower GC content and faster first phase kinetics than LS2, which deviated from the expected trend. Template LS2 st also fell outside the expected trend; although it did not have the weakest toehold, it failed to produce measurable amounts of trigger (Figure 4C). This was likely due to the small trigger size; at 8 nucleotides, polymerization or nicking may have been inefficient.

*Varying palindrome thermodynamics within templates*

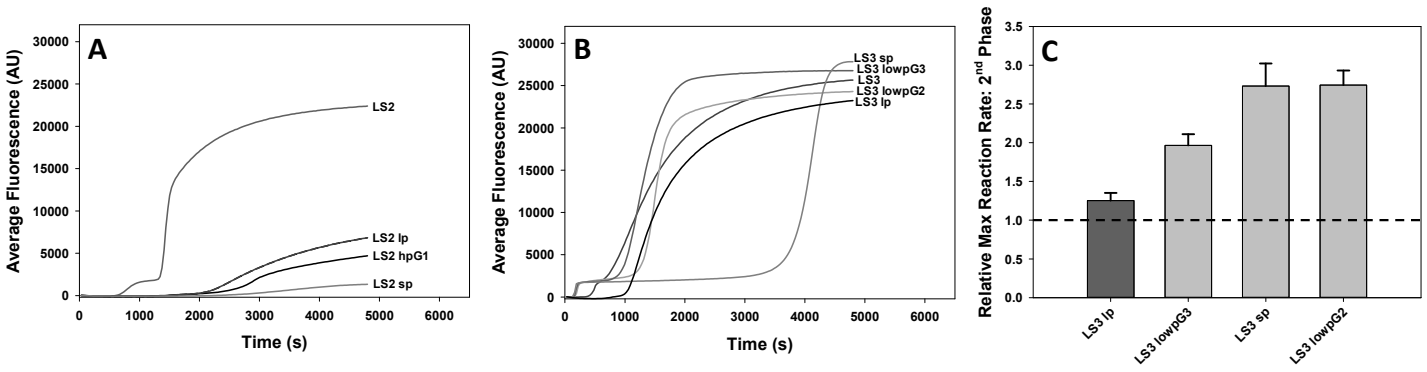


**Figure 5: Varying palindrome strength of looped templates.** A) Amplification curves of LS2 palindrome variants, with the strongest palindrome in black and weaker palindromes in lighter shades of grey. (B) Amplification curves of LS3 palindrome variants. (C) The templates shown in the bar graph are in order from strongest to weakest palindrome free energies, with darker grey signifying the templates with stronger palindromes than the base template. The relative maximum second phase reaction rate is the maximum slope (dF/dt) in the second rise divided by the maximum dF/dt in the second rise of the base template (LS3), which is a relative measure of the second phase reaction kinetics.

We varied the thermodynamics of the palindromic template and trigger region by varying the length or the GC content of the palindrome. Increasing the strength of the palindrome for template LS2 decreased the ability of the trigger to open

the stable template stem-loop structure (Figure 5A). This resulted in a slower reaction with subtle biphasic responses, making these templates ineffective as molecular switches. Reaction kinetics slowed dramatically when the free energy of the palindrome is lowered by replacing original palindrome base pairs with GC pairs (LS2 hpG1) or lengthening the palindrome (LS2 lp). Although decreasing the palindrome length favored trigger binding and subsequent loop opening, shortening the palindrome slowed the reaction kinetics. This is likely because template LS2sp was unusually short and paired with an 8 nucleotide trigger, which may have caused polymerization or nicking kinetics to be inefficient. All LS2 variant templates demonstrated altered kinetics, and their almost negligible first phases were difficult to accurately quantify.

Figure 5B & C demonstrates the effects of changing palindrome strength for the base template LS3. Decreasing the free energy of the palindrome caused the plateau phase to increase in length and the maximum reaction rate to increase in magnitude. Conversely, increasing the free energy of the palindrome nearly eliminates the first phase. This behavior supports the hypothesis that the binding of the palindromic region of the trigger to the long "poisoned" trigger-template hybrid facilitates template rescue.

*Varying loop thermodynamics within templates*

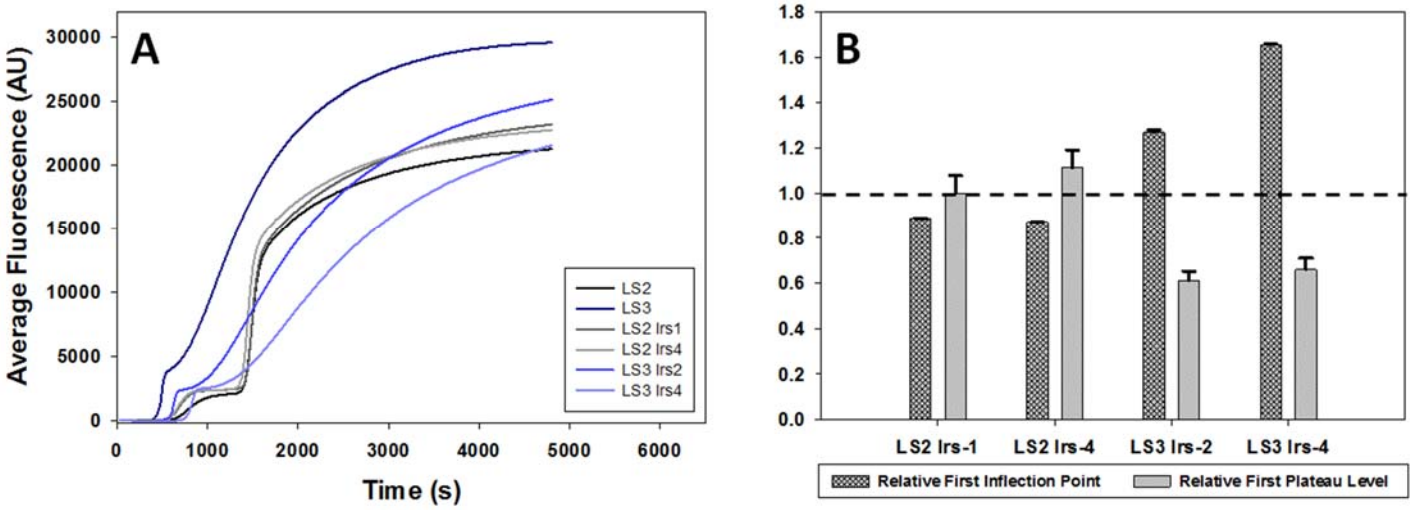


**Figure 6: Varying the loop strength of looped templates.** (A) Amplification curves of LS2 and LS3 loop variants, with the strongest loops for LS2 in black and the strongest loops for LS3 in dark blue. Weaker loops are indicated by lighter shades of grey or blue. (B) The templates shown in the bar graph are in order from strongest to weakest loop free energies with respect to the base template (LS2 and LS3). All lrs templates have weaker loop structures when compared to the base templates.

Figure 6 demonstrates another important source of kinetic variability: the strength of the loop. The free energy of the looped template structure was altered by adding long random sequences into the loop before the recognition site, which held the palindrome, toehold, and trigger sequences constant while varying stability of the template stem-loop structure. The only additional thermodynamic parameter this changed was the stability of the long trigger:template complex. For template LS2, decreasing the strength of the loop caused the loop to open faster, thereby decreasing the first inflection point as expected. This alteration did not have a large effect on the height of the first plateau. Surprisingly, decreasing the strength of the LS3 template loop slowed the first reaction phase (Figure 6B). We hypothesize that this phenomenon was caused by the increased stability of the long triggers, which included the original trigger sequence, the restriction site, and the long random sequences. These long triggers were more stable and more difficult to remove, which may have caused the lower product concentration at the reaction plateau seen in Figure 6B. LS3 templates had more stable loops, more stable trigger:template complexes, and stronger toeholds when compared to the LS2 family of templates. It is possible

that templates LS2 and LS3 operate in different reaction regimes with distinct dominant reaction pathways. Due to the many contributing mechanisms in the reaction, the template behavior could not be predicted by one parameter alone.

*Analyzing the ultrasensitive response of the second reaction phase*

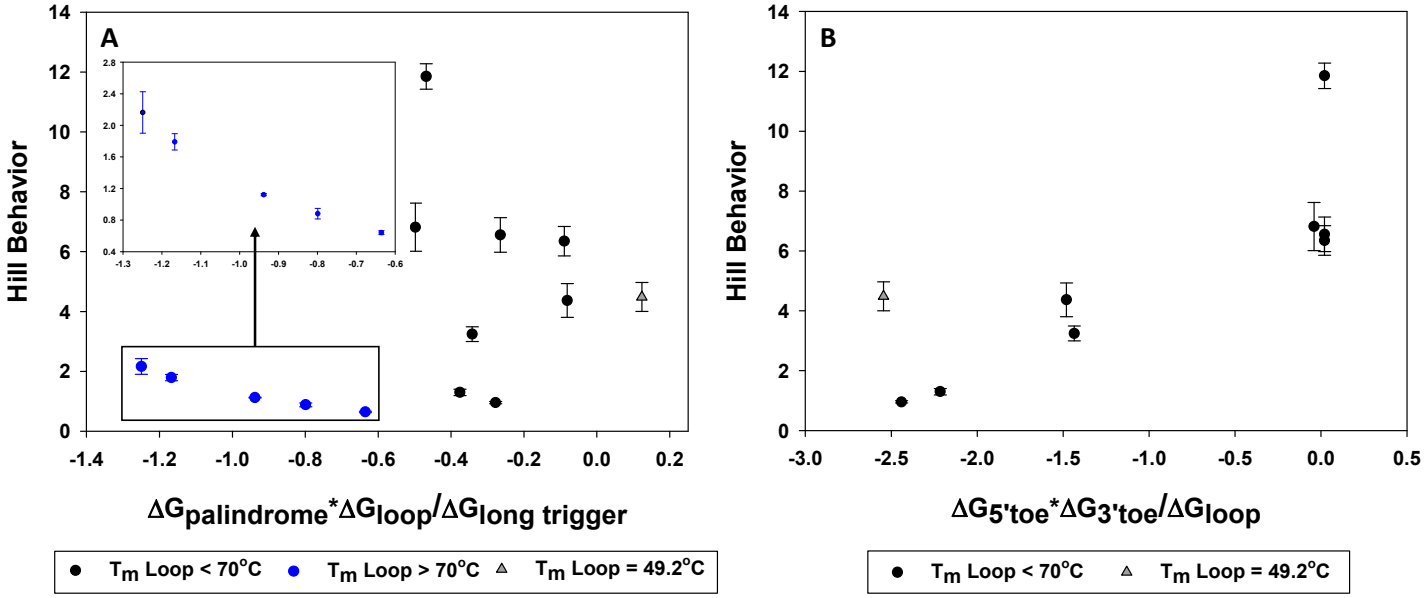


**Figure 7: Predicting the ultrasensitivity of the second phase kinetics using template thermodynamics.** We investigated two parameters that may predict ultrasensitivity based on two hypothesized mechanisms behind the Hill-type second phase kinetics. Hill behavior is quantified as the ratio between the maximum reaction rates in the second phase and first phase; a larger value would correspond to more pronounced Hill-type kinetics. (A) If the cooperativity of "poisoned" template removal contributed to Hill-type kinetics, then the parameter $L = \Delta G_{palindrome} * \Delta G_{loop}/\Delta G_{long\ trigger}$ would correlate with Hill-type behavior. This correlation is seen only in the strongest templates (Spearman R = -1), with the opposite relationship between Hill behavior and L than was expected for a cooperative effect. (B) If the cooperativity of trigger binding to the two open toeholds contributed to Hill-type kinetics, then the parameter $T = \Delta G_{5'toehold} * \Delta G_{3'toehold}/\Delta G_{loop}$ would correlate with Hill-type behavior. A correlation is seen in all templates that are stable at the reaction temperature and have a melting temperature < 70°C (Spearman R = 0.8539, p < 0.013).

We further analyzed DNA amplification kinetics for their Hill-like behavior to determine if ultrasensitive kinetics in the second phase could be rationally tuned using DNA association thermodynamics. The ratio of the maximum reaction rate in the second phase to the maximum reaction rate in the first phase approximates the Hill behavior of the reaction; a larger value would correspond with more pronounced Hill-type behavior (see Figure SI 4 for details of this calculation). We proposed two hypotheses to explain the ultrasensitive, Hill-like kinetics seen in the second phase of many reactions; we analyzed these hypotheses using two thermodynamic parameters that represent each proposed reaction mechanisms.

The first hypothesis was cooperative ultrasensitive kinetics were aided by multiple events that favor removal of the long trigger that has "poisoned" the template. These binding events include closing of the loop and binding of the trigger to the long inactive trigger (Figure 2A, panel 4). We characterized this reaction pathway by the parameter $L = \Delta G_{palindrome} * \Delta G_{loop}/\Delta G_{long\ trigger}$, with higher negative values favoring displacement of a long inactive trigger molecule. If the long inactive trigger molecule was easily displaced, the cooperative effects of loop closure and trigger association would not have been as pronounced. Therefore, if long trigger removal was contributing to ultrasensitive kinetics, the Hill behavior would have been more pronounced for less negative values of L. Figure 7A shows the relationship between apparent Hill behavior and the parameter L. Templates with the greatest loop stability (> 70°C) showed the opposite trend than expected for a cooperative effect; the second phase was faster for a more easily displaced long trigger and the reaction showed minimal Hill behavior (Figure 7A, blue circles). The data suggested that these reactions were struggling to overcome thermodynamic penalties such as long trigger removal. There was no evidence that the inactive long trigger removal contributed to the ultrasensitive second phase kinetics in these templates, although

there was clear evidence that the parameter L was correlated with relative reaction kinetics for the most stable templates. With one exception (Figure 7A, grey triangle), the remaining templates also had stable loops at the 55°C reaction temperature; these templates did not show Hill behavior that correlated with the parameter L (Figure 7A, black circles).

The second hypothesis was multiple trigger binding sites on the template favor opening of the thermodynamically stable loop at high trigger concentrations, which would produce ultrasensitive kinetics through positive cooperativity. We characterized this pathway by the parameter $T = \Delta G_{5',toehold} * \Delta G_{3',toehold} / \Delta G_{loop}$, with a more negative value favoring trigger binding and an open template. If the loop was easily opened, then a cooperative effect would not have been as advantageous to shift the template to an open configuration. If the looped structure could efficiently open within the range of product trigger concentrations, then ultrasensitive Hill behavior would be more pronounced for less negative values of T. Figure 7B shows the relationship between Hill behavior and the parameter T, which showed a correlation between T and Hill behavior (Spearman R = 0.8569, $p < 0.013$). This correlation supported the hypothesis that toehold cooperativity significantly contributed to ultrasensitive kinetics in the second phase for these templates. This theory had precedent in literature; structure-switching receptors with multiple ligand binding sites were known to give Hill-type outputs in response to a ligand[29]. The association of one trigger was thermodynamically unfavorable when compared to the loop structure (Table SI 2), but upon association the trigger will open the loop structure and switch the receptor to a binding competent state (Figure 2A, panel 1).

## Conclusions

DNA association thermodynamics roughly correlate with the main reaction features: first phase reaction kinetics, first plateau, and second phase reaction kinetics. The strength of the toehold and trigger association with the template both correlate with kinetics in the first phase, suggesting that the probability of opening the stable looped template structure will largely determine the first phase output. The ability of the template and triggers to remove long triggers appear to be a secondary factor in determining the first phase kinetics. We hypothesize that the accumulation of "poisoned" templates with bound unextendible long triggers may slow the reaction. These long triggers also appear to determine the plateau level: strongly bound long triggers will freeze the reaction faster than weakly bound long triggers, lowering the trigger concentration seen at the plateau. Second phase kinetics are more complex. Templates with a strong loop configuration did not show strong Hill-type behavior and rapid second phase kinetics. It is possible that these template populations never favor the open, binding competent structure over the closed loop structure at the produced trigger concentrations. Templates with a loop melting temperature below 70°C show faster kinetics in the second phase when toeholds are thermodynamically weaker when compared to the strength of the loop. When the template melts below the reaction temperature, these correlations no longer apply but the reaction remains biphasic. These observations provide important design considerations to tune the reaction output during each phase.

Future applications of this biphasic DNA amplification reaction require further investigation and optimization. Due to the multiple contributing reaction pathways, the relationship between DNA association thermodynamics and reaction output is currently defined by imperfect correlations. Currently, reactions must be screened after template design. Reaction design would be aided by mathematical modeling of reaction kinetics and a full mechanistic understanding of the reaction phases. As with many isothermal amplifications such as EXPAR, this reaction also produces non-specific amplification in the absence of an oligonucleotide trigger occurring at long reaction times. Non-specific amplification will increase the limit of detection and can decrease the experimental robustness. Adding ssDNA binding proteins and carbon sheets[30] or other small molecules[31] can decrease non-specific amplification in EXPAR reactions, and would likely also be applicable in this reaction. Degradation of the reaction product was previously used to create a bistable switch from an EXPAR-type reaction[14], and could be extended to suppress non-specific amplification or create threshold-based detection for targets above a chosen concentration. Inhibition or degradation or reaction products could also create a true bistable switch that could turn "off" and "on" with tunable ultrasensitive kinetics.

We have demonstrated a novel new biosensor with a two-stage output based on the concentration of a released trigger molecule. The biphasic DNA amplification reaction is a simple, one-step isothermal amplification reaction; reactions of

this type have gained popularity as they do not require temperature cycling and therefore require less energy, hardware, and time[32,33]. We have described a general reaction design framework to rationally tune first phase kinetics and second phase ultrasensitive DNA output. This chemistry can be tuned by changing the thermodynamics of the looped template and reporter DNA molecules. In the future, we will expand the capabilities of the reaction: trigger DNA oligonucleotides can be created by proteins[34-38], genomic bacterial DNA[39], viral DNA[40], microRNA[41], or mRNA[42], making the biphasic DNA amplification reaction broadly applicable to a variety of target molecules. When combined with digital (single molecule) amplification, this technique has the potential to be quantitative. The biphasic nature of this reaction makes it well suited for recognition of low-concentration molecules in biological samples, DNA logic gates, and other molecular recognition systems.

**Acknowledgements:** This publication was supported by the National Center For Advancing Translational Sciences of the National Institutes of Health under Award Number UL1 TR002319 and the Montana Research and Economic Development Seed Funds.

## Supplementary Info

### Materials and Methods

*Reagents*

UltraPure™ Tris-HCl pH 8.0, RNase free EDTA, RNase free $MgCl_2$, RNase free KCl, Novex™ TBE Running Buffer (5X), 2X TBE-Urea Sample Buffer, Novex™ TBE-Urea Gels, 15%, SYBR® Gold Nucleic Acid Gel Stain, and SYBR® Green II RNA Gel Stain were purchased from Thermo Fisher Scientific (Waltham, MA). Nuclease-free water and oligo length standard 10/60 were purchased from Integrated DNA Technologies, Inc. (Coralville, IA). Nt.BstNBI nicking enzyme, *Bst* 2.0 WarmStart® DNA Polymerase, 10x ThermoPol I Buffer, dNTPs, BSA, and 100 mM $MgSO_4$ were purchased from New England Biolabs (Beverly, MA).

Oligonucleotides were ordered from two different sources to avoid trigger contamination in templates. Desalted amplification templates were purchased from Integrated DNA Technologies (Coralville, IA) suspended in IDTE Buffer at a concentration of 100 µM. Templates were modified with an amino group on the 3' end to prevent template extension. All desalted trigger oligonucleotides were purchased from Eurofins Genomics (Louisville, KY) suspended at a concentration of 50 µM in TE Buffer. Triggers were diluted in nuclease-free water in a separate room to prevent contamination.

*Template design and thermodynamics*

Thermodynamics of the template stem loops were determined using the Mfold web server[43], an open source software that uses empirical free energies of DNA hybridization[44] that have been corrected for salt concentration[45] (http://unafold.rna.albany.edu/?q=mfold). The free energies of association between the template and trigger, template and elongated trigger, product dimers, and double stranded templates were determined using the DINAMelt application, two-state melting (http://unafold.rna.albany.edu/?q=DINAMelt/Two-state-melting). To determine the free energy of toehold association, the software input was the sequence of the toehold and the toehold reverse compliment. All settings used were kept at the default software parameters, except for temperature (55°C) and salt concentration ($[Na^+]$ = 60mM, $[Mg^{++}]$ = 6mM).

*Biphasic Amplification Reactions*

The amplification reaction mixture contained 1x ThermoPol I Buffer [20 mM Tris-HCl (pH 8.8), 10 mM $(NH_4)_2SO_4$, 10 mM KCl, 2 mM $MgSO_4$, 0.1% Triton® X-100], 25 mM Tris-HCl (pH 8), 6 mM $MgSO_4$, 50 mM KCl, 0.5 mM each dNTP, 0.1 mg/mL

BSA, 0.2 U/µL Nt.BstNBI, and 0.0267 U/µL *Bst* 2.0 WarmStart® DNA Polymerase. *Bst* 2.0 WarmStart® DNA polymerase is inactive below 45°C; this decreases non-specific amplification before reaction initiation and theoretically increases experimental reproducibility. Templates were diluted in nuclease-free water and added at a final concentration of 100 nM. SYBR Green II (10,000x stock in DMSO) was added to the reaction mixture to a final concentration of 5x. Reactions were prepared at 4°C, and triggers and templates were handled in separate hoods to prevent contamination. Triggers were diluted in nuclease-free water and added to positive samples to a final concentration of 10 pM unless otherwise indicated; negative controls contained no trigger. For each experiment, two controls were prepared: a no-template control (NTC) sample containing no template, and a no-enzyme control sample containing no enzymes. Reactions were run in triplicate 20 µL volumes. Fluorescence readings were measured using a BioRad CFX Connect Thermocycler (Hercules, CA). Measurements were taken every 20 seconds with a 12 second imaging step. Reactions were run for either 150 or 300 cycles of 32 seconds at 55°C. The mixture was heated to 80°C for 20 minutes to deactivate enzymes, followed by 10°C for five minutes to cool the samples. Completed reactions were stored at -20°C for further analysis.

*Product quantification*

NanoDrop 3300 Fluorospectrometer (Thermo Scientific, Wilmington, DE) was used for measuring the reaction product concentrations. The standards (ssDNA oligos, Eurofins Genomics, Louisville, KY) and the reaction products were diluted in 1X TE buffer (1mM Tris-HCl, 0.5 mM EDTA) if needed. Nucleic acid stains were diluted in 1X TE Buffer. 1X SYBR® Gold Nucleic Acid Gel Stain (for low concentration samples) or 2.5X SYBR® Green II RNA Gel Stain (for high concentration samples), and 1.2 µL of the sample were brought to a final volume of 12 µL with 1X TE buffer. The standards were prepared in the same way as the reaction products with the addition of mock reaction product (reaction components without enzymes or trigger) and triggers diluted in 1X TE Buffer. The excitation of the samples was conducted using blue light (470 ± 10 nm) with autogain on. The fluorescence peaks of the dyes were determined to be 512 nm for SYBR® Green II RNA Gel Stain and 536 nm for SYBR® Gold Nucleic Acid Gel Stain for the specific salt conditions, and the average fluorescence value at the fluorescence spectrum peak was used to determine the product concentrations of the reaction products. 1X TE buffer was used as the blank measurement and 5 replicates for each sample were measured.

*PAGE analysis of reaction products*

Novex™ TBE Running Buffer (5X) was diluted to a 1X final concentration in milliQ ultrapure water. Templates, triggers, reaction products and ladder were diluted to concentrations specified in 2X TBE-Urea Sample Buffer. Oligo length standard 10/60 was used as the ladder. The working solution for loading the samples to the gel was prepared using 1uL of the sample, 1X TBE-Urea Sample Buffer and 1X TE buffer to bring the final volume to 6 µL. The samples were denatured by incubating at 80˚C in a thermocycler (iCycler, Bio-Rad, Hercules, CA) for 5 minutes and immediately put on ice for storage until loading to the gel. The 1X Novex™ TBE Running Buffer was heated to approximately 50˚C before filling the Bolt® Mini Gel Tank, purchased from Thermo Fisher Scientific (Waltham, MA). Novex™ TBE-Urea Gels, 15%, 10 or 15 well, were used according to the manufacturer's protocol with the voltage set to 180V for approximately 25 minutes. Gel staining solution was prepared by diluting 10,000X SYBR® Gold Nucleic Acid Gel Stain to 1X in 1X Novex™ TBE Running Buffer. Immediately after the run, gels were stained and imaged using UltraBright LED Transilluminator (Maestrogen, Atkinson, NH) at a 470nm wavelength excitation.

*Data analysis*

Real-time reaction traces were analyzed with custom software using Matlab (Natick, MA). Inflection points were defined as the peaks in the first derivate of the fluorescence with respect to time. To determine exact inflection points, the top of the peak was fit to a quadratic function $dF/dt = at^2+bt+c$ where F is fluorescence and t is time. The inflection point was defined as the zero of the second derivative ($t_{IF} = 2at+b$). The first plateau was defined as the fluorescence corresponding to the time of the lowest point between the first and second peaks in the first derivative. The maximum reaction rates were defined as the top of the peaks in the first derivative (maximum dF/dt). See Figure SI 4 for more details on analysis of the real-time reaction traces.

The ratios between maximum reaction rates, plateaus, and inflection points were calculated from two experiments with three experimental replicates each. When appropriate, data from two experiments were averaged using a weighted average[46] ($x_{wav}$) from experimental averages ($x_i$) standard deviations ($\sigma_i$):

$$x_{wav} = \frac{\sum w_i x_i}{\sum w_i}, w_i = \frac{1}{\sigma_i^2}, and\ \sigma_{wav}^2 = \frac{1}{\sum w_i}$$

Spearman's rank-order correlations and p-values were determined using the function "corr" with the type selected as "Spearman" in Matlab (Natick, MA).

Standard curves relating fluorescence to trigger DNA concentration were fit to a simple linear regression model using the statistical computing software RStudio. The mean trigger concentration predictions of the unknowns were obtained using the "inverse.predict" function of RStudio, under the package "chemCal". Standard deviations were computed using the function "stdev" in the electronic spreadsheet program Microsoft Excel. Standard error from the predicted concentration was converted to standard deviation and the cumulative standard deviation of the trigger DNA concentration was calculating using the formula[47]:

$$SD_{total} = \sqrt{SD_{prediction}{}^2 + SD_{sample\ mean\ of\ the\ replicates}{}^2}$$

| Template Name | Sequence | Trigger |
|---|---|---|
| LS2 | 5' - TCCGGA *GAAT* TAATGACTCT TCCGG *A GAAT* - 3' $NH_2$ | 5' - ATTCTCCGGA - 3' |
| LS3 | 5' - CGCGCG *GTTTGG* TAATGACTCT CGCGCG *GTTTGG* - 3' $NH_2$ | 5' - CCAAACCGCGCG - 3' |
| Long random sequence in the loop - Increase the loop opening ΔG, Decrease the elongated Trigger:Template ΔG | | |
| LS2 lrs-1 | 5' - TCCGGA *GAAT* TAATGACTCT GCTT TCCGG *A GAAT*- 3' $NH_2$ | 5' - ATTCTCCGGA - 3' |
| LS2 lrs-4 | 5' - TCCGGA *GAAT* TAATGACTCT GCTTAGTCAG TCCGG *A GAAT* - 3' $NH_2$ | 5' - ATTCTCCGGA - 3' |
| LS3 lrs-2 | 5' - CGCGCG *GTTTGG* TAATGACTCT GCTTAG CGCGCG *GTTTGG* - 3' $NH_2$ | 5' - CCAAACCGCGCG - 3' |
| LS3 lrs-4 | 5' - CGCGCG *GTTTGG* TAATGACTCT ACTTGGCTTA CGCGCG *GTTTGG* - 3' $NH_2$ | 5' - CCAAACCGCGCG - 3' |
| Vary palindrome length and GC content - change palindrome ΔG and elongated Trigger:Template ΔG | | |
| LS3 lp* | 5' - CGCGCGCG GTTTG- TAATGACTCT CGCGCGCG *GTTTG*- - 3' $NH_2$ | 5' - CAAACCGCGCGCG - 3' |
| LS3 lowpG3 | 5' - TCCGGA *GTTTGG* TAATGACTCT TCCGG *A GTTTGG* - 3' $NH_2$ | 5' - CCAAACTCCGGA - 3' |
| LS3 sp | 5' - CGCG *GTTTGG* TAATGACTCT CGCG *GTTTGG* - 3' $NH_2$ | 5' - CCAAACCGCG - 3' |
| LS3 lowpG2 | 5' - TAGCTA *GTTTGG* TAATGACTCT TAGCTA *GTTTGG* - 3' $NH_2$ | 5' - CCAAACTAGCTA - 3' |
| LS2 hpG1*†† | 5'- GCCGGC *GAAT* TAATGACTCT GCCGGC *GAAT* - 3' $NH_2$ | 5' - ATTCGCCGGC - 3' |
| LS2 lp*†† | 5' - GTCCGGAC *GAAT* TAATGACTCT GTCCGGAC *GAAT* - 3' $NH_2$ | 5' - ATTCGTCCGGAC - 3' |
| LS2 sp† | 5' - CCGG *GAAT* TAATGACTCT CCGG *GAAT* - 3' $NH_2$ | 5' - ATTCCCGG - 3' |
| Vary toehold length and GC content - change toehold ΔG and elongated Trigger:Template ΔG | | |
| LS3 lt1 | 5' - CGCGCG *GTTTGGACG* TAATGACTCT CGCGCG *GTTTGGACG* - 3' $NH_2$ | 5' - CGTCCAAACCGCGCG - 3' |
| LS3 htG†† | 5' - CGCGCG *GTGCGG* TAATGACTCT CGCGCG *GTGCGG* - 3' $NH_2$ | 5' - CCGCACCGCGCG - 3' |
| LS3 lowtG | 5' - CGCGCG *GTTTAT* TAATGACTCT CGCGCG *GTTTAT* - 3' $NH_2$ | 5' - ATAAACCGCGCG - 3' |
| LS2 htG2 | 5' - TCCGGA *GCGC* TAATGACTCT TCCGG *A GCGC* - 3' $NH_2$ | 5' - GCGCTCCGGA - 3' |
| LS2 lt3 | 5' - TCCGGA *GAATGATC* TAATGACTCT TCCGG *A GAATGATC* - 3' $NH_2$ | 5' - GATCATTCTCCGGA - 3' |
| LS2 st‡ | 5' - TCCGGA *GA* TAATGACTCT TCCGG *A GA* - 3' $NH_2$ | 5' - TCTCCGGA - 3' |
| LS2 lowtG | 5' - TCCGGA *TAAT* TAATGACTCT TCCGG *A TAAT* - 3' $NH_2$ | 5' - ATTATCCGGA - 3' |
| No 5' toehold - lock the 5' toehold using added nucleotides in the loop - decrease loop ΔG and elongated Trigger:Template ΔG, remove cooperative binding of trigger | | |
| LS2 no5'*†† | 5' - TCCGGA GAAT TAATGACTCT ATTC TCCGG *A GAAT* - 3' $NH_2$ | 5' - ATTCTCCGGA - 3' |
| LS2 no5' lrs3*†† | 5' - TCCGGA GAAT TAATGACTCT GTATAGCT ATTC TCCGG A *GAAT* - 3' $NH_2$ | 5' - ATTCTCCGGA - 3' |
| Linear Templates | | |
| Ran2** | 5' - GGGGAAATAG GTGAGACTCT GGGGAAATAG - 3' NH2 | 5' - CTATTTCCCC - 3' |
| EXPAR1** | 5' - CTCACGCTAC GGACGACTCT CTCACGCTAC - 3' $PO_3$ | 5' - GTAGCGTGAG - 3' |

† = did not enter high gain phase, †† = did not have a measureable low gain phase, * = ab initio synthesis after approximately 4800 s,
** = ab initio synthesis after approximately 1800s, ‡ = no amplification

**Table SI 1: Template and trigger sequences**

| Template Name | 3' toe ΔG, kcal/mol | 5' toe ΔG, kcal/mol | Palindrome ΔG, kcal/mol | Palindrome $T_m$ | Loop ΔG, kcal/mol | Loop $T_m$ | Trigger: Template ΔG, kcal/mol | Trigger: Template $T_m$ | Elongated Trigger: Template ΔG, kcal/mol | Elongated Trigger: Template $T_m$ |
|---|---|---|---|---|---|---|---|---|---|---|
| LS2 | -0.4 | 0.2 | -3.9 | 27°C | -1.6 | 67.1°C | -6.9 | 47.5°C | -13.0 | 65.5°C |
| LS3 | -2.0 | -2.0 | -5.9 | 46.4°C | -3.66 | 76.7°C | -11.6 | 65.4°C | -18.5 | 74.7°C |
| Long random sequence in the loop - Increase the loop opening ΔG, Decrease the elongated trigger:template ΔG | | | | | | | | | | |
| LS2 lrs-1 | -0.4 | 0.2 | -3.9 | 27°C | -1.14 | 63.7°C | -6.9 | 47.5°C | -16.8 | 70.8°C |
| LS2 lrs-4 | -0.4 | 0.2 | -3.9 | 27°C | -0.49 | 58.8 | -6.9 | 47.5°C | -21.4 | 74.5 |
| LS3 lrs-2 | -2.0 | -2.0 | -5.9 | 46.4°C | -3.25 | 73.5°C | -11.7 | 65.6°C | -24.0 | 79.1°C |
| LS3 lrs-4 | -2.0 | -2.0 | -5.9 | 46.4°C | -2.8 | 71.2°C | -11.9 | 66.1°C | -26.0 | 79°C |
| Vary palindrome length and GC content - change palindrome ΔG and elongated trigger:template ΔG | | | | | | | | | | |
| LS3 lp* | -0.7 | -0.7 | -9.1 | 61.6°C | -6.97 | 86.5°C | -13.5 | 69.9°C | -20.3 | 77.0°C |
| LS3 lowpG3 | -2.8 | -2.0 | -3.9 | 27.0°C | -1.35 | 65.4°C | -8.9 | 56.7°C | -15.4 | 69.2°C |
| LS3 sp | -2.0 | -2.0 | -2.7 | 19.4°C | -0.46 | 58.9°C | -8.4 | 55.0°C | -15.3 | 70.0°C |
| LS3 lowpG2 | -2.8 | -2.0 | -2.2 | 12.7°C | 0.73 | 49.2°C | -6.8 | 49.3°C | -13.0 | 64.3°C |
| LS2 hpG1*†† | 0.2 | 0.2 | -5.2 | 41.3°C | -3.56 | 78.9°C | -9.1 | 58.1°C | -16 | 71.9°C |
| LS2 lp*†† | 0.2 | 0.2 | -5.1 | 43.9°C | -3.56 | 73.7°C | -9.1 | 57.6°C | -16 | 70.5°C |
| LS2 sp† | 0.2 | 0.2 | -2.2 | 11.8°C | -0.15 | 56.4°C | -5.6 | 38.3°C | -12.4 | 65.1°C |
| Vary toehold length and GC content - change toehold ΔG and elongated trigger:template ΔG | | | | | | | | | | |
| LS3 lt1 | -5.2 | -5.2 | -5.9 | 46.4°C | -3.45 | 75.3°C | -14.8 | 71.8°C | -21.7 | 77.8°C |
| LS3 htG†† | -4.3 | -4.3 | -5.9 | 46.4°C | -3.66 | 76.7°C | -13.9 | 72.4°C | -20.8 | 78.9°C |
| LS3 lowtG | -0.5 | -0.5 | -5.9 | 46.4°C | -3.66 | 76.7°C | -10.1 | 61.1°C | -17 | 72.8°C |
| LS2 htG2 | -3.6 | -2.4 | -3.9 | 27.0°C | -1.56 | 67.1°C | -9.8 | 60.6°C | -16.2 | 72.0°C |
| LS2 lt3 | -3.4 | -2.8 | -3.9 | 27.0°C | -1.14 | 63.7°C | -9.4 | 58.6°C | -16 | 70.3°C |
| LS2 st‡ | 0.1 | 1 | -3.9 | 27.0°C | -1.67 | 68.0°C | -5.9 | 40.4°C | -12.4 | 65.2°C |
| LS2 lowtG | 0.4 | 0.4 | -4.0 | 30.7°C | -1.48 | 66.6°C | -5.8 | 42.2°C | -11.9 | 63.0°C |
| No 5' toehold - lock the 5' toehold using added nucleotides in the loop - decrease loop ΔG and elongated trigger:template ΔG, remove cooperative binding of trigger | | | | | | | | | | |
| LS2 no5'*†† | -0.4 | n/a | -3.9 | 27.0°C | -4.05 | 73.9°C | -6.9 | 47.5°C | -15 | 67.4°C |
| LS2 no5' lrs3*†† | -0.4 | n/a | -3.9 | 27.0°C | -3.31 | 70.3°C | -6.9 | 47.5°C | -20.4 | 72.1°C |
| Linear templates | | | | | | | | | | |
| Ran2** | n/a | n/a | n/a | n/a | n/a | n/a | -5.1 | 41.2°C | -13.9 | 67.4°C |
| EXPAR1** | n/a | n/a | n/a | n/a | n/a | n/a | -6.5 | 47.4°C | -16.7 | 73.3°C |

**Table SI 2: Template Thermodynamics**

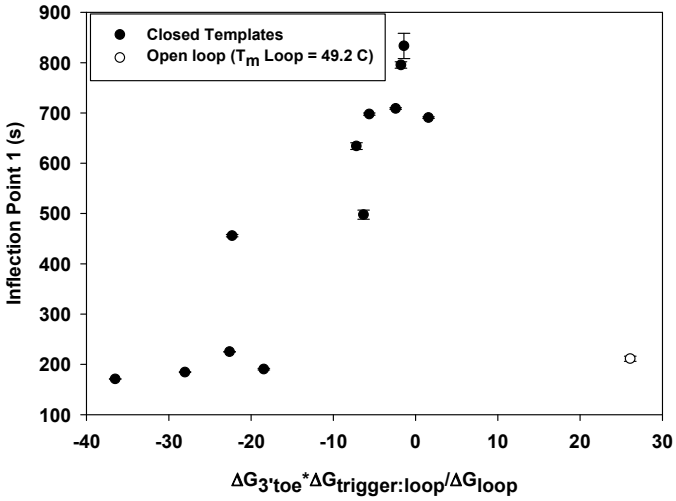


**Figure SI 1: Correlation between kinetics of the first phase and the opening of the looped template.** The 3' toehold region dominates kinetics of loop opening[48] to form an amplifiable molecule; the strength of the trigger:template association will contribute to loop opening and the ability of the loop to stay open, while the strength of the template structure obstructs loop opening. Therefore, a more negative value of the ratio $\Delta G_{3'toe} * \Delta G_{trigger:loop} / \Delta G_{loop}$ should favor trigger binding, faster kinetics, and a smaller inflection point. This trend is seen in the data: the inflection point increases as the ratio approaches zero. The open circle represents a template that does not form a loop at the reaction temperature of 55°C, and was thus not included when calculating the Spearman Rho (R = 0.8022, $p < 0.0016$).

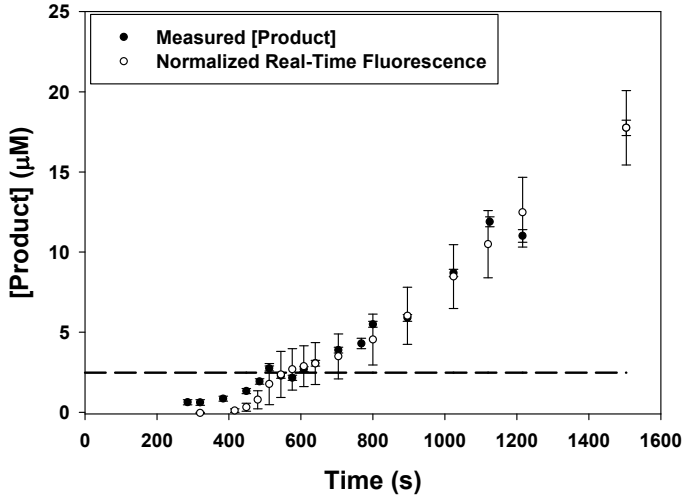


**Figure SI 2: Product quantification time course.** The filled circles show product concentration in LS3 reactions that were removed and quantified at different times. The open circles are an average of n = 18 runs of LS3 reaction fluorescence taken in a real-time PCR instrument, which have been normalized to match the final 1504 second time point. The dotted line shows the level of the first plateau (2.5 ± 0.2 μM), averaged over 3 data points. Given that the ratio of plateau levels of the template LS3 lrs-4 to the template LS3 is 0.66 (Figure 4), the hypothetical plateau of LS3 lrs-4 is 1.6 μM; this is in good agreement with the 1 μM estimated plateau given in in Figure 3.

| Template | Palindrome ΔG (kcal/mol) | Estimated [Product] (μM) | SD (μM) |
|---|---|---|---|
| LS3 lp* | -9.1 | 27.7 | ± 4.2 |
| LS3 | -5.9 | 80.9 | ± 4.6 |
| LS3 lrs-2 | -5.9 | 76.5 | ± 4.5 |
| LS3 lrs-4 | -5.9 | 70.9 | ± 4.5 |
| LS3 lt1 | -5.9 | 90.7 | ± 5.0 |
| LS3 htG | -5.9 | 95.9 | ± 4.9 |
| LS3 lowtG | -5.9 | 63.9 | ± 4.2 |
| LS2 hpG1* | -5.2 | 5.3 | ± 1.0 |
| LS2 lp* | -5.1 | 12.2 | ± 1.0 |
| LS2 | -3.9 | 82.0 | ± 7.5 |
| LS2 lrs-1 | -3.9 | 80.1 | ± 7.5 |
| LS2 lrs-4 | -3.9 | 87.4 | ± 8.7 |
| LS2 lt3 | -3.9 | 114.3 | ± 7.8 |
| LS2 htG2 | -3.9 | 116.9 | ± 9.5 |
| LS2 lowtG | -3.9 | 83.0 | ± 7.5 |
| LS2 no5'* | -3.9 | 7.8 | ± 1.0 |
| LS2 no5' lrs3* | -3.9 | 33.4 | ± 1.1 |
| LS3 lowpG3 | -3.9 | 80.4 | ± 4.5 |
| LS3 sp | -2.7 | 91.7 | ± 5.4 |
| LS3 lowpG2 | -2.2 | 73.2 | ± 4.6 |
| EXPAR1** | n/a | 5.6 | ± 0.3 |

*The reaction time was shorter than 9632s to quantify products before *ab intio* synthesis. (4800s)
**The reaction time was shorter than 9632s to quantify products before *ab intio* synthesis. (1800s)

**Table SI 3: Endpoint concentrations of trigger, quantified at 9632 seconds unless otherwise indicated.**

| Template | Late Phase Inflection Point Experiment 1 | Late Phase Inflection Point Experiment 2 |
|---|---|---|
| LS2 hpG1* | 869 ± 1760 | 484 ± 1790 |
| LS2 lp* | -1493 ± 1151 | 741 ± 1865 |
| LS2 sp | -1134 ± 752 | ± |

**Table SI 4: Late phase amplification due to *ab initio* synthesis have unpredictable rise times.** The above templates had late phase amplification >4800 s with inflection points that were not correlated with original trigger concentration and not predictable within experiments. If a second phase does not have *ab initio* synthesis in PAGE gel analysis, the second inflection point is consistent within and between experiments. The above templates all showed ab initio synthesis in PAGE gel analysis of reaction products (Figure SI 3).

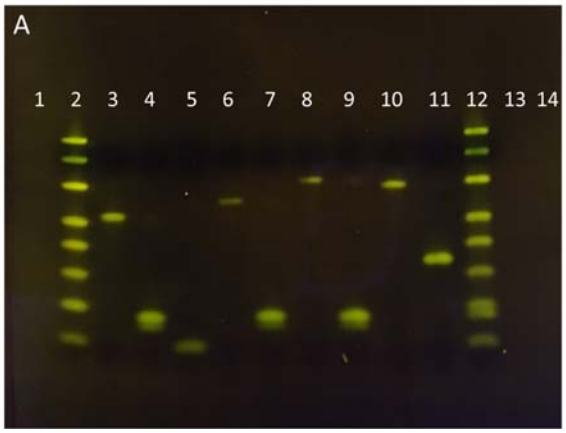


| Well number | Sample name | Sample concentration |
|---|---|---|
| 1 | Empty | - |
| 2 | Ladder | 5.00 ng/µl |
| 3 | LS2 template | 0.25 µM |
| 4 | LS2 product | 3.28 µM |
| 5 | LS2 trigger | 5.00 µM |
| 6 | LS2 lrs-1 template | 0.10 µM |
| 7 | LS2 lrs-1 product | 3.20 µM |
| 8 | LS2 lrs-4 template | 0.10 µM |
| 9 | LS2 lrs-4 product | 3.50 µM |
| 10 | LS2 lt-3 template | 0.25 µM |
| 11 | LS2 lt-3 product | 3.81 µM |
| 12 | LS2 lt-3 trigger + Ladder | 1.00 µM , 5.00 ng/µl |
| 13 | Empty | - |
| 14 | Empty | - |

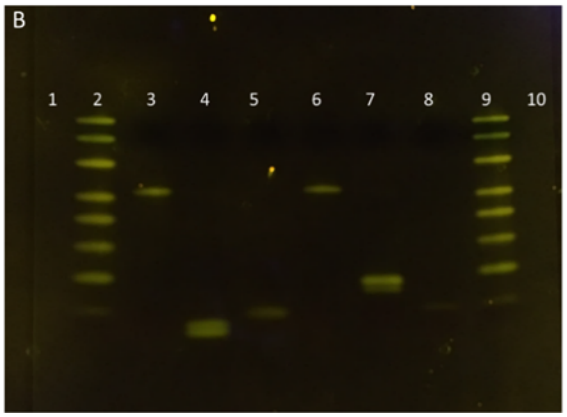


| Well number | Sample name | Sample concentration |
|---|---|---|
| 1 | Empty | - |
| 2 | Ladder | 5.00 ng/µl |
| 3 | LS2 htG-2 template | 0.25 µM |
| 4 | LS2 htG-2 product | 2.92 µM |
| 5 | LS2 htG-2 trigger | 2.50µM |
| 6 | LS2 lowtG template | 0.25 µM |
| 7 | LS2 lowtG product | 2.77 µM |
| 8 | LS2 lowtG trigger | 5.00 µM |
| 9 | Ladder | 5.00 ng/µl |
| 10 | Empty | - |

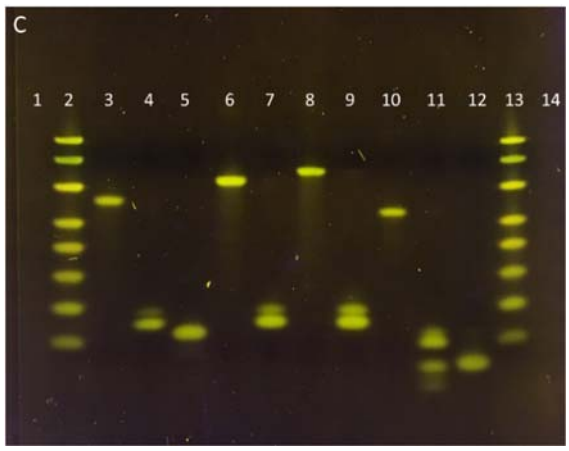


| Well number | Sample name | Sample concentration |
|---|---|---|
| 1 | Empty | - |
| 2 | Ladder | 5.00 ng/µl |
| 3 | LS3 template | 0.50 µM |
| 4 | LS3 product | 2.70 µM |
| 5 | LS3 trigger | 5.00 µM |
| 6 | LS3 lrs-2 template | 1.00 µM |
| 7 | LS3 lrs-2 product | 7.65 µM |
| 8 | LS3 lrs-4 template | 1.00 µM |
| 9 | LS3 lrs-4 product | 7.09 µM |
| 10 | LS3 htG template | 0.50 µM |
| 11 | LS3 htG product | 4.79 µM |
| 12 | LS3 htG trigger | 2.50 µM |
| 13 | Ladder | 5.00 ng/µl |
| 14 | Empty | - |
| 15 | Empty | - |

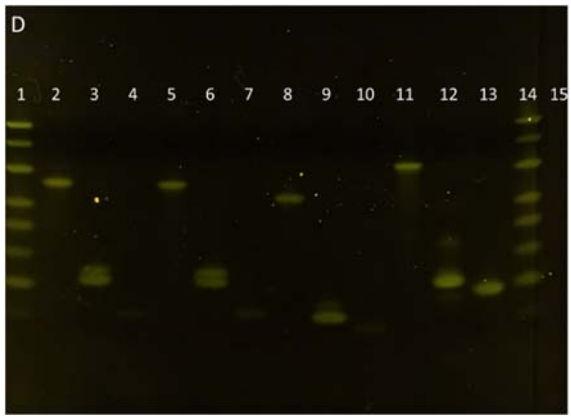


| Well number | Sample name | Sample concentration |
|---|---|---|
| 1 | Empty | - |
| 2 | Ladder | 5.00 ng/µl |
| 3 | LS3 lowpG-2 template | 0.50 µM |
| 4 | LS3 lowpG-2 product | 3.66 µM |
| 5 | LS3 lowpG-2 trigger | 10.00 µM |
| 6 | LS3 lowpG-3 template | 0.50 µM |
| 7 | LS3 lowpG-3 product | 4.02 µM |
| 8 | LS3 lowpG-3 trigger | 10.00 µM |
| 9 | LS3 sp template | 0.50 µM |
| 10 | LS3 sp product | 4.59 µM |
| 11 | LS3 sp trigger | 20.00 µM |
| 12 | LS3 lt-1 template | 0.50 µM |
| 13 | LS3 lt-1 product | 3.02 µM |
| 14 | LS3 lt-1 trigger | 2.50 µM |
| 15 | Empty | - |

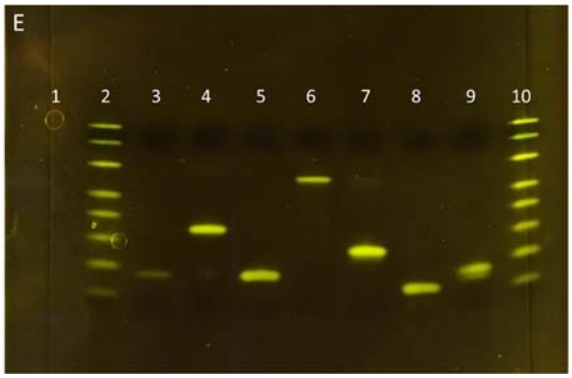


| Well number | Sample name | Sample concentration |
|---|---|---|
| 1 | Empty | - |
| 2 | Ladder | 5.00 ng/µl |
| 3 | LS2 lt-3 trigger | 2.50 µM |
| 4 | LS2 lt-3 product | 5.72 µM |
| 5 | LS2 lt-3 trigger | 2.50 µM |
| 6 | LS3 lowtG template | 0.50 µM |
| 7 | LS3 lowtG product | 12.77 µM |
| 8 | LS3 lowtG trigger | 5.00 µM |
| 9 | LS2 product | 3.28 µM |
| 10 | Ladder | 5.00 ng/µl |

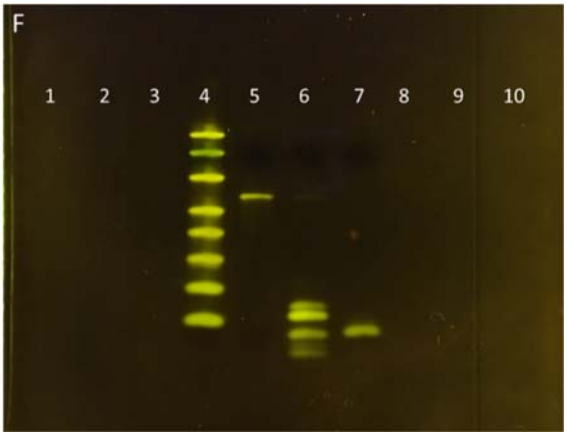


| Well number | Sample name | Sample concentration |
|---|---|---|
| 1 | Empty | - |
| 2 | Empty | - |
| 3 | Empty | - |
| 4 | Ladder | 0.05 ng/uL |
| 5 | LS3 htG template | 0.50 µM |
| 6 | LS3 htG reaction product | 4.79 µM |
| 7 | LS3 htG trigger | 5.00 µM |
| 8 | Empty | - |
| 9 | Empty | - |
| 10 | Empty | - |

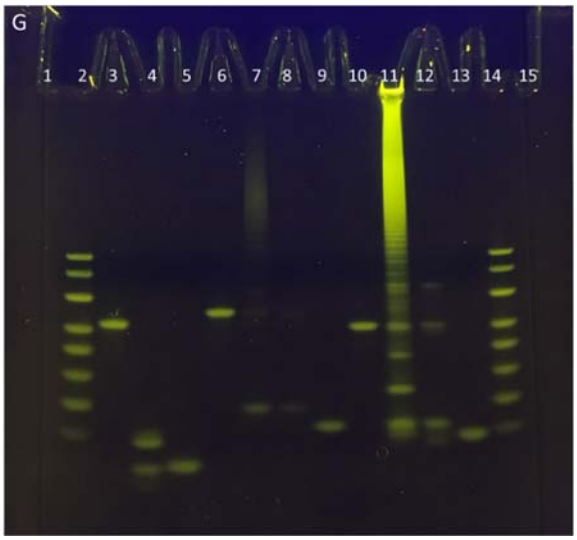


| Well number | Sample name | Sample concentration |
|---|---|---|
| 1 | Empty | - |
| 2 | Ladder | 5.00 ng/µl |
| 3 | LS3 htG template | 0.50 µM |
| 4 | LS3 htG product | 4.79 µM |
| 5 | LS3 htG trigger | 2.50 µM |
| 6 | LS2 lp template | 0.50 µM |
| 7 | LS2 lp product | N/A |
| 8 | LS2 lp product* | 2.43 uM |
| 9 | LS2 lp trigger | 2.50 µM |
| 10 | LS2 hpG-1 template | 0.50 µM |
| 11 | LS2 hpG-1 product | N/A |
| 12 | LS2 hpG-1 product* | 5.33 µM |
| 13 | LS2 hpG-1 trigger | 5.00 µM |
| 14 | Ladder | 5.00 ng/µl |
| 15 | Empty | - |

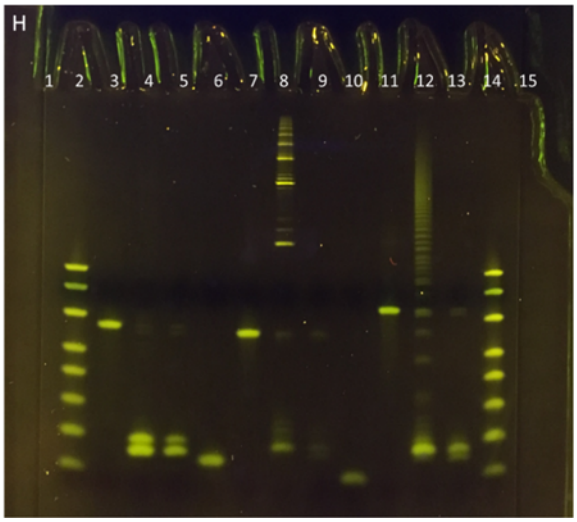


| Well number | Sample name | Sample concentration |
|---|---|---|
| 1 | Empty | - |
| 2 | Ladder | 5.00 ng/µl |
| 3 | LS3 lp ptemplate | 0.50 µM |
| 4 | LS3 lp product | N/A |
| 5 | LS3 lp product* | 2.77 µM |
| 6 | LS3 lp trigger | 2.50 µM |
| 7 | LS2 no5' template | 0.50 µM |
| 8 | LS2 no5' product | N/A |
| 9 | LS2 no5' product* | 0.78 µM |
| 10 | LS2 trigger | 50 µM |
| 11 | LS2 no5 lrs-3 template | 0.50 µM |
| 12 | LS2 no5 lrs-3 product | N/A |
| 13 | LS2 no5 lrs-3 product* | 3.34 µM |
| 14 | Ladder | 5.00 ng/µl |
| 15 | Empty | - |

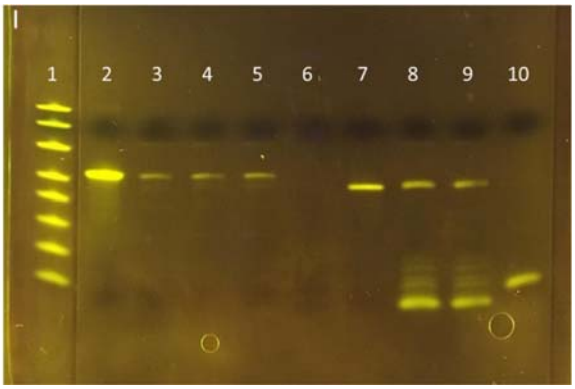


| Well number | Sample name | Sample concentration |
|---|---|---|
| 1 | Ladder | 5.00 ng/µl |
| 2 | Ran 2 template | 0.50 µM |
| 3 | Ran 2 product-1** | - |
| 4 | Ran 2 product-2** | - |
| 5 | Ran 2 product-3** | - |
| 6 | Ran 2 trigger | 5.00 µM |
| 7 | EXPAR1 template | 0.50 µM |
| 8 | EXPAR1 product-1** | 5.58 uM |
| 9 | EXPAR1 product-2** | 5.58 uM |
| 10 | EXPAR1 trigger | 5.00 µM |

**Figure SI 3: PAGE gel analysis.** Templates, triggers, and reaction products are shown for all biphasic DNA amplification reactions. All looped templates form products in the same size range as their triggers, with no evidence of *ab initio* synthesis before 4800s. Templates that showed multiple large bands characteristic of *ab initio* synthesis were rerun for shorter reaction durations: * = *ab initio* synthesis detected after 9632 s, rerun for 4800 s. ** = *ab initio* synthesis detected after 4800 s, rerun for 1800 s. (A) LS2 with added long random sequences and long toehold templates, triggers, and reaction products. (B) LS2 high and low toehold ΔG templates, triggers, and reaction products. (C) LS3 with added long random sequences and LS3 high toehold ΔG templates, triggers, and reaction products. (D) LS3 long toehold, LS3 short palindrome, LS3 low palindrome ΔG templates, triggers, and reaction products. (E) LS2 long toehold, LS3 low toehold ΔG templates, triggers, and reaction products. (F) LS3 high toehold ΔG templates, triggers, and reaction products. (G) LS2 long palindrome and high palindrome ΔG templates, triggers, and reaction products. This gel also contains a repeat of the LS3 high toehold ΔG reaction products seen in gel F. (H) LS3 long palindrome and LS2 templates with no open 5' toehold templates, triggers, and reaction products. (I) Traditional linear EXPAR templates, triggers, and reaction products.

We have hypothesized that an elongated trigger forms due to trigger dimerization and subsequent polymerase extension, which would lead to the main end product of the reaction to be the elongated trigger (Figure 2, panel 5). The PAGE gels in Figure SI 3 show that most of the reaction products contain two different bands; one of the bands matches the hypothesized size of the elongated trigger and the other differs by one or two nucleotides from the size of the elongated trigger. The bands that are one or two nucleotides shorter than the elongated trigger (in the case of LS3 lowpG-2, LS2 lowpG-3 and LS3 sp templates, Figure SI 3D) may be formed when the nicking enzyme cleaves the complementary template strand by displacing the polymerase before it is done with full polymerization of the template[49]. These short oligonucleotides would still have the palindrome sites that would cause the production of elongated triggers, but they

would be one or two nucleotides shorter than the original elongated trigger. Most of the template products have a second band that is one or two nucleotides longer than the elongated trigger band, and in some cases, there is only one band that is the same size with the hypothesized elongated trigger band (LS2 lt-3 (Figure SI 3A) and LS3 lowtG templates(Figure SI 3E)). Other templates do not have a product that exactly matches the hypothesized elongated trigger size. Instead, they have products that match the size of their triggers. For the templates L LS2 hpG-1 (Figure SI 3G) and LS3 lp (Figure SI 3H), it is possible they do not have elongated trigger products because their short reaction time to prevent ab initio synthesis may not allow the elongation step to fully occur. The templates and the long triggers that contain a restriction endonuclease sequence are not seen in most of the gel images. Most of the products were diluted between 1:10 and 1:40 to increase resolution of the high concentrated products, such that the low concentrated products cannot be detected. Products with a visible template band were diluted [x]; these were poorly amplified samples with low reaction product concentrations (Table SI 3). They also did not contain a visible long trigger band.

Another important observation from these gel images is that some of the templates have *ab initio* synthesis after 1800s (traditional EXPAR templates EXPAR1, Ran2 (Figure SI 3I)) or 4800s (LS2 hpG1, LS2 lp (Figure SI 3G), LS3 lp, LS2 no5', LS2 no5' lrs3 (Figure SI 3H)), characterized by many bands above the initial trigger size[22]. *Ab initio* synthesis is seen when the ratio of the free energy of a template loop to the free energy of the template:trigger hybrid is high and reaction kinetics are slow (Figure SI 6); definitive biphasic DNA amplification outputs did not yield ab initio synthesis before 9632s. We hypothesize that when the loop spends more time in the closed configuration (the higher the ratio on the y axis), the polymerase is less occupied and is more likely to engage in *ab initio* synthesis. If the reaction time is reduced from 9632s to 4800s, we did not detect *ab initio* synthesis in the DNA biphasic amplification reactions.

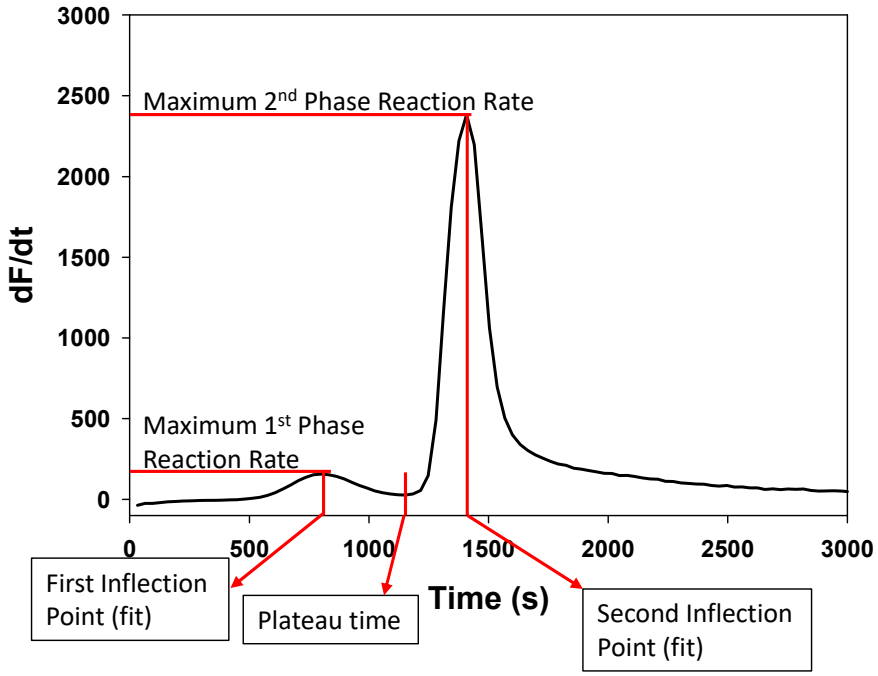


**Figure SI 4: Retrieving reaction parameters.** The parameters calculated for each amplification reaction were: first and second inflection points (seconds), maximum reaction rates for the first and second phase (d(Fluorescence)/dt), and first plateau time (seconds). The level of the first plateau (in fluorescent units) was determined using the value of the fluorescence at the plateau time.

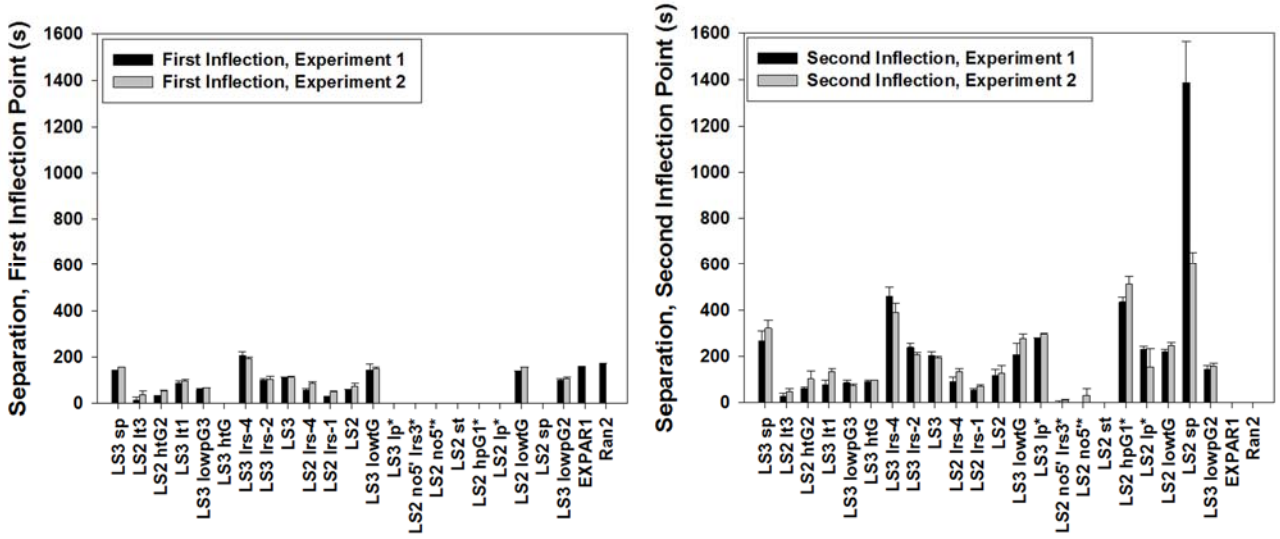


**Figure SI 5**: **Separation of inflection points between negative and positive controls.** All reactions initiated with 10pM of trigger DNA had inflection points that were distinct from negative controls with no initial trigger present, except for templates with bound 5' toeholds (LS2 no5' and LS2 no5' lrs3). LS2 st did not amplify, and all other templates showing no separation did not have a measureable inflection point for the given reaction phase. Experimental replicates (n=3) had standard deviations shown by the error bars; between experiments data would sometimes fall outside of the standard deviations for experimental replicates. For this reason, data for each experiment is shown separately. The templates are shown in order, with $\Delta G_{trigger:loop} * \Delta G_{3'toe}/\Delta G_{loop}$ from lowest to highest. Starred templates gave *ab initio* synthesis after 4800s.

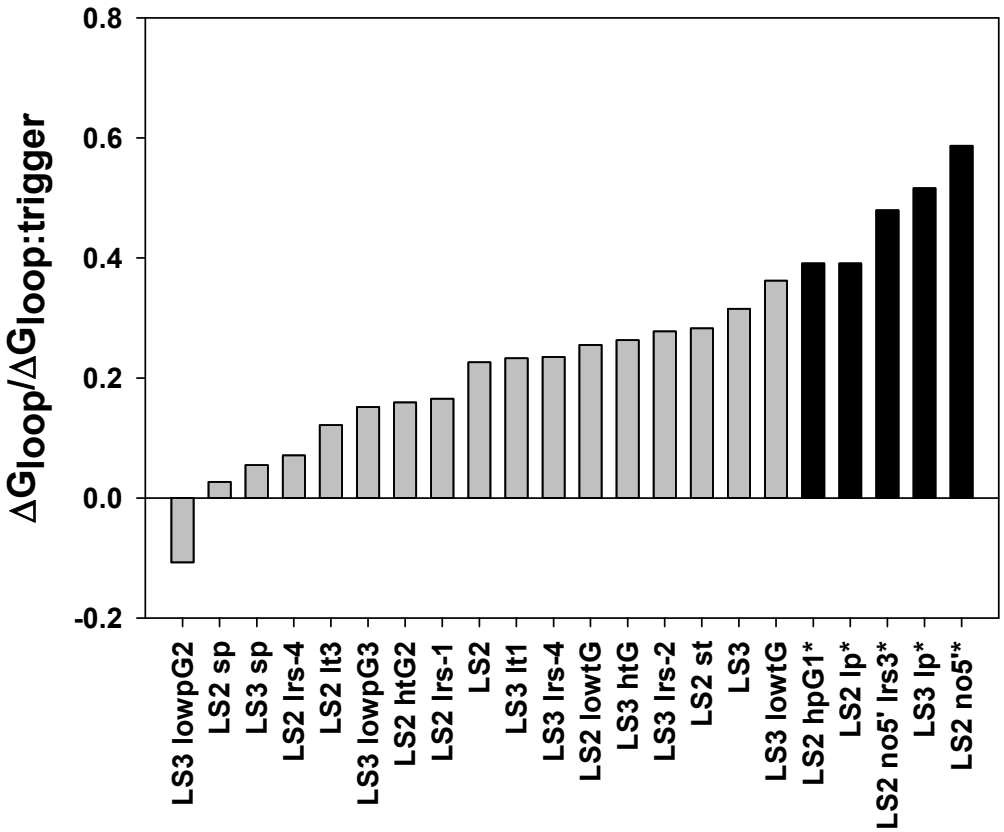


**Figure SI 6:** Starred templates show ab initio synthesis after 4800s; these templates also have the highest delGloop/delGtrigger ratio and are therefore the hardest to open at the reaction temperature.

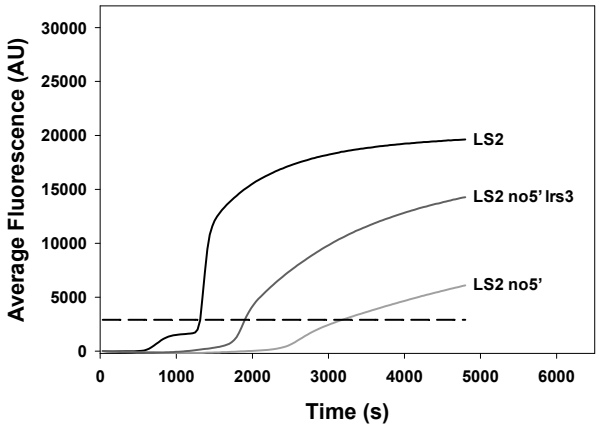


**Figure SI 7: Effect of removing the 5' toehold.** Templates were designed with extra nucleotides that bound the 5' toehold. This slowed kinetics due to an increase in loop stability (LS2>LS2 no5' lrs3 > LS2 no5'). These templates still appear to enter the second phase of amplification, showing that the looped template alone is sufficient to rescue the reaction from the first plateau.

References

1. Ferrell, J.E. Tripping the switch fantastic: how a protein kinase cascade can convert graded inputs into switch-like outputs. *Trends in biochemical sciences* **21**, 460-466 (1996).
2. Zhang, Q., Bhattacharya, S. & Andersen, M.E. Ultrasensitive response motifs: basic amplifiers in molecular signalling networks. *Open biology* **3**, 130031 (2013).
3. Buchler, N.E. & Louis, M. Molecular titration and ultrasensitivity in regulatory networks. *Journal of molecular biology* **384**, 1106-1119 (2008).
4. Mukherji, S*., et al.* MicroRNAs can generate thresholds in target gene expression. *Nature genetics* **43**, 854-859 (2011).
5. Huang, C.-Y. & Ferrell, J.E. Ultrasensitivity in the mitogen-activated protein kinase cascade. *Proceedings of the National Academy of Sciences* **93**, 10078-10083 (1996).
6. Notides, A.C., Lerner, N. & Hamilton, D.E. Positive cooperativity of the estrogen receptor. *Proceedings of the National Academy of Sciences* **78**, 4926-4930 (1981).
7. Meinke, M.H., Bishop, J.S. & Edstrom, R.D. Zero-order ultrasensitivity in the regulation of glycogen phosphorylase. *Proceedings of the National Academy of Sciences* **83**, 2865-2868 (1986).
8. Ha, S. & Ferrell, J. Thresholds and ultrasensitivity from negative cooperativity. *Science* **352**, 990-993 (2016).
9. Adair, G.S. The hemoglobin system VI. The oxygen dissociation curve of hemoglobin. *Journal of Biological Chemistry* **63**, 529-545 (1925).
10. Plaxco, K.W. & Soh, H.T. Switch-based biosensors: a new approach towards real-time, in vivo molecular detection. *Trends in Biotechnology* **29**, 1-5.
11. Simon, A.J., Vallée-Bélisle, A., Ricci, F. & Plaxco, K.W. Intrinsic disorder as a generalizable strategy for the rational design of highly responsive, allosterically cooperative receptors. *Proceedings of the National Academy of Sciences* **111**, 15048-15053 (2014).
12. Simon, A.J., Vallée-Bélisle, A., Ricci, F., Watkins, H.M. & Plaxco, K.W. Using the Population-Shift Mechanism to Rationally Introduce “Hill-type” Cooperativity into a Normally Non-Cooperative Receptor. *Angewandte Chemie* **126**, 9625-9629 (2014).
13. Cornell, B.A., Braach-Maksvytis, V., King, L. & Osman, P. A biosensor that uses ion-channel switches. *Nature* **387**, 580 (1997).
14. Montagne, K., Gines, G., Fujii, T. & Rondelez, Y. Boosting functionality of synthetic DNA circuits with tailored deactivation. *Nature Communications* **7**, 13474 (2016).
15. Zuo, X*., et al.* A target-responsive electrochemical aptamer switch (TREAS) for reagentless detection of nanomolar ATP. *Journal of the American Chemical Society* **129**, 1042-1043 (2007).
16. Vallée-Bélisle, A., Ricci, F. & Plaxco, K.W. Thermodynamic basis for the optimization of binding-induced biomolecular switches and structure-switching biosensors. *Proceedings of the National Academy of Sciences* **106**, 13802-13807 (2009).
17. Tyagi, S. & Kramer, F.R. Molecular beacons: probes that fluoresce upon hybridization. *Nature biotechnology*, 303-308 (1996).
18. Zhou, Y*., et al.* A dumbbell probe-mediated rolling circle amplification strategy for highly sensitive microRNA detection. *Nucleic acids research* **38**, e156-e156 (2010).
19. Kelley, S.O. What Are Clinically Relevant Levels of Cellular and Biomolecular Analytes? *ACS Sensors* **2**, 193-197 (2017).
20. Rissin, D.M*., et al.* Single-molecule enzyme-linked immunosorbent assay detects serum proteins at subfemtomolar concentrations. *Nature biotechnology* **28**, 595-599 (2010).
21. Qian, J*., et al.* Sequence dependence of isothermal DNA amplification via EXPAR. *Nucleic acids research* **40**, e87-e87 (2012).
22. Tan, E*., et al.* Specific versus Nonspecific Isothermal DNA Amplification through Thermophilic Polymerase and Nicking Enzyme Activities†. *Biochemistry* **47**, 9987-9999 (2008).

23. Van Ness, J., Van Ness, L.K. & Galas, D.J. Isothermal reactions for the amplification of oligonucleotides. *Proceedings of the National Academy of Sciences* **100**, 4504-4509 (2003).
24. Fujii, T. & Rondelez, Y. Predator–prey molecular ecosystems. *ACS nano* **7**, 27-34 (2012).
25. Padirac, A., Fujii, T., Estévez-Torres, A. & Rondelez, Y. Spatial waves in synthetic biochemical networks. *Journal of the American Chemical Society* **135**, 14586-14592 (2013).
26. Zambrano, A., Zadorin, A.S., Rondelez, Y., Estévez-Torres, A. & Galas, J.C. Pursuit-and-Evasion Reaction-Diffusion Waves in Microreactors with Tailored Geometry. *The Journal of Physical Chemistry B* **119**, 5349-5355 (2015).
27. Baccouche, A., Montagne, K., Padirac, A., Fujii, T. & Rondelez, Y. Dynamic DNA-toolbox reaction circuits: a walkthrough. *Methods* **67**, 234-249 (2014).
28. Lage, J.M.*, et al.* Whole genome analysis of genetic alterations in small DNA samples using hyperbranched strand displacement amplification and array–CGH. *Genome Research* **13**, 294-307 (2003).
29. Ricci, F., Vallée-Bélisle, A., Simon, A.J., Porchetta, A. & Plaxco, K.W. Using Nature's "Tricks" To Rationally Tune the Binding Properties of Biomolecular Receptors. *Accounts of Chemical Research* **49**, 1884-1892 (2016).
30. Wang, J.*, et al.* Exponential amplification of DNA with very low background using graphene oxide and single-stranded binding protein to suppress non-specific amplification. *Microchimica Acta* **182**, 1095-1101 (2015).
31. Mok, E., Wee, E., Wang, Y. & Trau, M. Comprehensive evaluation of molecular enhancers of the isothermal exponential amplification reaction. *Scientific reports* **6**(2016).
32. McCalla, S.E. & Tripathi, A. Microfluidic reactors for diagnostics applications. *Annual review of biomedical engineering* **13**, 321-343 (2011).
33. Li, J. & Macdonald, J. Advances in isothermal amplification: novel strategies inspired by biological processes. *Biosensors and Bioelectronics* **64**, 196-211 (2015).
34. Zhang, Z.-z. & Zhang, C.-y. Highly Sensitive Detection of Protein with Aptamer-Based Target-Triggering Two-Stage Amplification. *Analytical Chemistry* **84**, 1623-1629 (2012).
35. Tang, W.*, et al.* Sensitive detection of tumor cells based on aptamer recognition and isothermal exponential amplification. *RSC Advances* **6**, 89888-89894 (2016).
36. Qiu, T.*, et al.* Label-free, homogeneous, and ultrasensitive detection of pathogenic bacteria based on target-triggered isothermally exponential amplification. *RSC Advances* **6**, 62031-62037 (2016).
37. Nutiu, R. & Li, Y. Structure-switching signaling aptamers. *Journal of the American Chemical Society* **125**, 4771-4778 (2003).
38. Wieland, M., Benz, A., Haar, J., Halder, K. & Hartig, J.S. Small molecule-triggered assembly of DNA nanoarchitectures. *Chemical Communications* **46**, 1866-1868 (2010).
39. Roskos, K.*, et al.* Simple System for Isothermal DNA Amplification Coupled to Lateral Flow Detection. *PLoS ONE* **8**, e69355 (2013).
40. Tan, E., Erwin, B., Dames, S., Voelkerding, K. & Niemz, A. Isothermal DNA amplification with gold nanosphere-based visual colorimetric readout for herpes simplex virus detection. *Clinical chemistry* **53**, 2017-2020 (2007).
41. Zhang, X., Liu, C., Sun, L., Duan, X. & Li, Z. Lab on a single microbead: an ultrasensitive detection strategy enabling microRNA analysis at the single-molecule level. *Chemical Science* **6**, 6213-6218 (2015).
42. Zhao, Y., Zhou, L. & Tang, Z. Cleavage-based signal amplification of RNA. *Nat Commun* **4**, 1493 (2013).
43. Zuker, M. Mfold web server for nucleic acid folding and hybridization prediction. *Nucleic acids research* **31**, 3406-3415 (2003).
44. SantaLucia, J. A unified view of polymer, dumbbell, and oligonucleotide DNA nearest-neighbor thermodynamics. *Proceedings of the National Academy of Sciences* **95**, 1460-1465 (1998).
45. Peyret, N. *Prediction of nucleic acid hybridization: parameters and algorithms*, (Wayne State University Detroit, 2000).
46. Taylor, J. *Introduction to error analysis, the study of uncertainties in physical measurements*, (1997).
47. Ellison, S. & Williams, A. Eurachem/CITAC guide: Quantifying uncertainty in analytical measurement, (2012). *Available from* www. *eurachem. org* (2015).

48. Srinivas, N.*, et al.* On the biophysics and kinetics of toehold-mediated DNA strand displacement. *Nucleic acids research* **41**, 10641-10658 (2013).

49. Van Ness, J., Van Ness, L.K. & Galas, D.J. Isothermal reactions for the amplification of oligonucleotides. *Proc Natl Acad Sci U S A* **100**, 4504-4509 (2003).